Iranian Journal of Catalysis 6(5), 2016, 415-421

IRANIAN JOURNAL OF CATALYSIS

Enhanced photocatalytic activity of sonochemical derived ZnO via the co-doping process

Maryam Bordbar[a,*], Solmaz Forghani-pilerood[b], Ali Yeganeh-Faal[b]

[a]*Department of Chemistry, Faculty of Science, University of Qom, Qom, Iran.*

[b]*Faculty of Science, Payame Noor University, Tehran, Iran.*

Received 1 May 2016; received in revised form 10 June 2016; accepted 14 July 2016

ABSTRACT

In the present study, Co-ZnO and Co-Ni-ZnO nanoparticles were synthesized by sonochemical methods and the structural and optical properties were investigated through Fourier Transform Infrared spectroscopy (FTIR), UV-Vis spectroscopy, Field Emission Scanning Electron Microscopy (FE-SEM), X-Ray Diffraction (XRD), and Photoluminescence spectroscopy (PL) methods. Morphology of nanoparticles obtained a small granular shape with an average crystallite size of 60 nm. In addition, the direct band gap was calculated using Tauc's approach. Comparing with pure ZnO, the band gap of the doped-ZnO NPs is smaller and depends on the type of dopants. Moreover, photocatalytic activity of all samples was investigated by the degradation of methyl orange (MO) dye under UV irradiation in an aqueous medium. Co-Ni-ZnO possesses excellent photocatalytic activity for the degradation of MO when compared to Co-ZnO and ZnO. In addition, the photocatalytic activity of Co-ZnO improves in the presence of nickel dopant. Moreover, the photocatalyst could be reused for four times without remarkable loss of its activity.

***Keywords**: (Co, Ni)-doped ZnO, Band gap, Photocatalytic activity, Sonochemical method.*

1. Introduction

Dyes widely used in textiles, plastics, paper, and rubber industries, have led to water pollution due to the release of the colored and toxic wastewater into water bodies [1]. The treatment of dye waste effluents is usually inefficient, costly and non-destructive or just transfers pollution from water to another phase.

Recently, semiconductor nanoparticles such as TiO_2, ZnO and WO_3 have been used as photo-catalysis for complete removal of dye pollutants [2-10] Zinc oxide (ZnO) [10,11] is an inexpensive wide band gap semiconductor (3.37 eV) and its photocatalytic mechanism is similar to that of TiO_2 [4]. Therefore, a great deal of attention has been focused on ZnO nanostructures. Photocatalytic activity property of ZnO nanostructures is limited by fast recombination of the photogenerated electron-hole, and low adsorption ability. Numerous efforts such as type of synthesis method, metal ion doping and coupling with other semiconductors have been carried out [12-15].

*Corresponding author email: m.bordbare@gmail.com
Tel.: +98 25 3210 3792; Fax: +98 25 3285 0953

In doped ZnO samples, the addition of carriers seems to increase the carrier concentration and enhance photocatalytic activity. [16] One common feature was that, in all samples, secondary phases are formed at high dopant concentration and at high annealing temperatures. Therefore, it was proposed that the possible effects of co-doping, i.e. simultaneous doping of ZnO with two or more transition metal ions [17,18]. However, the photocatalytic activity of transition metal doped (co-doped) semiconductors is higher than that of single element doped semiconductors.

Dong *et al*. [17] studied the photocatalytic activities of Al and Er doped ZnO under visible light. They have reported that that Er-Al co-doped ZnO showed much enhanced photocatalytic activity to the pristine ZnO in the degradation of MO. Rajarajan *et al*. [4] examined the photocatalytic performance of Ni and Th co-doped ZnO nanoparticles for the degradation of methylene blue dye and showed that Ni-Th-ZnO possesses excellent photocatalytic activity for the degradation of MB when compared to that of Ni-ZnO, Th-ZnO, ZnO and TiO_2.

Ni^{2+} modified semiconductors effectively eliminate the electron hole recombination during photocatalysis. In addition, compared with undoped ZnO, the photocatalytic properties of the Co-doped ZnO due to larger content of oxygen vacancies or defects which produced by doping Co^{2+}, have improve greatly [19]. Previous works have demonstrated the influence of Co^{2+} and Ni^{2+} ion doping on the optical properties of semiconducting oxides, providing the formation of multi-emission centers in the final materials, and promoting a charge-transfer state just below the band-gap energy [20], But they did not study the photocatalytic activity of (Ni, Co) co-doped ZnO.

Although most of the literature focused on Ni-doped ZnO [21] or Co-doped ZnO [22], the photocatalytic activity of ZnO co-doped using Co and Ni has not been explored. It is expected that co-doping with Ni and Co can increase the photocatalytic activity by reducing electron-hole recombination rate.

In this paper, we described a simple sonochemical synthesis of ZnO, cobalt doped ZnO (Co-ZnO) and (Cobalt, Nickel) co-doped ZnO (Co-Ni ZnO) nanoparticles, starting from aqueous zinc acetate as the source of zinc, and aqueous solution of NaOH as the source of oxygen without using any capping molecule. Furthermore, the effect of co-doping of Ni and Co, on the structure, optical and photocatalytic activity properties of ZnO has been studied in detail.

2. Experimental

2.1. Materials and equipment

Zinc acetate dehydrate ($Zn(Ac)_2.2H_2O$), sodium hydroxide (NaOH) and nickel nitrate tetrahydrate ($Ni(NO_3)_2.4H_2O$) were obtained from Merck Chemical Company. The sample structures were characterized by XRD patterns obtained on a Philips model X'PertPro X-ray diffractometer using Cu Kα radiation (λ= 1.54 Å), while the morphologies of the synthetic samples were investigated by field emission scanning electron microscopy (FESEM; TESCAN-MIRA3) equipped with an Oxford Inca Energy Dispersive X-ray detector. The optical absorptions of the samples were obtained using a Shimadzu UV-2500 spectrophotometer equipped with quartz cell of 1 cm path length. Fourier transform infrared spectra (FTIR) of the samples were recorded using a Jasco model 4200 FTIR spectrophotometer over the frequency range of 400-4000 cm^{-1} using KBr as the diluent. The room temperature photoluminescence (RT-PL) measurements were performed on a Cary Eclipse fluorescence spectrophotometer with a wavelength of 325 nm as the excitation source. In order to evaluate the photocatalytic activity of the samples, methyl orange (MO) degradation was evaluated as follows: Before the illumination, a 5 ppm solution of MO was magnetically stirred in the dark for 1 h to ensure the establishment of absorption equilibrium of methyl orange on the photocatalyst sample surfaces. Following this, the suspension was irradiated under a 50 W low-pressure Hg lamp. UV-Vis absorption spectra were recorded at different times to calculate MO concentrations

2.2. Sample preparation

2.2.1. ZnO NPs

Samples were synthesized by a simple sonochemical method using a sonochemical bath. The procedure was as follows: At first, 25 mL of a 0.1 M aqueous solution of zinc acetate in a beaker on an ice bath was kept in a sonication bath (28 KHz, 340 W). Then, 100 mL of a 0.1 M aqueous solution of sodium hydroxide was added to this solution dropwise for about 45-50 min. Finally, the white precipitate was filtered, then washed with distilled water and dried in an oven at 60ºC for 1 h. In the presence of ultrasound, the following reaction occurs:

$$Zn^{2+} + 4OH^- \overset{)))}{\longleftrightarrow} [Zn(OH)_4]^{2-}$$

$$2\,[Zn(OH)_4]^{2-} \longleftrightarrow 2ZnO + 4H_2 + 3O_2$$

2.2.2. Co-ZnO and Co-Ni- ZnO NPs

All the steps in the synthesis of Co-ZnO and Co-Ni-ZnO NPs were similar to those for ZnO NPs, but 0.0125 mmol of cobalt acetate ([Co]/[Zn]%= 0.50) for the Co-ZnO 0.00625 mmol cobalt acetate and 0.00625 mmol nickel acetate ([Co]/[Zn]%= 0.25 and [Ni]/[Zn]%= 0.25) for the Co-Ni-ZnO sample were added to aqueous zinc acetate solution in the first step.

3. Results and Discussion

3.1. Sample characterization

FE-SEM images were used to describe the morphologies. Fig. 1 shows the FE-SEM images of ZnO nanostructure prepared using the sonochemical method.

FE-SEM image reveals that the obtained particles are uniform and have spherical shapes with the diameters varying between 65 to 70 nm [23,24] (see particle size distribution, Fig. 1). The composition of ZnO, Co-ZnO and Co-Ni ZnO NPs was determined by the elemental dispersion analysis using X-ray (EDX) measurements. The EDX results confirm the presence and uniform distribution of the elements zinc, cobalt, nickel and oxygen (Fig. 2 and Table 1).

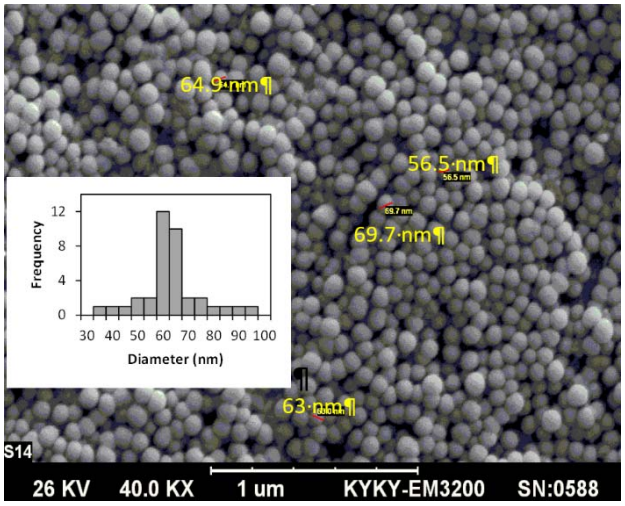

Fig. 1. SEM images of ZnO sample prepared by sono-chemical method.

The characteristic functional groups of samples were investigated using FTIR spectroscopy at room temperature in the range of 4000-400 cm^{-1} and the results are shown in Fig. 3.

The broad peak observed in 460-560 cm^{-1} is the combination of Zn-O vibrations. Moreover, in undoped and doped samples, no obvious changes can be seen in FTIR spectra. It is worth mentioning that Co and Ni atoms were successfully incorporated into the crystal lattice of ZnO. Therefore, it is reasonable to conclude that synthetic product has no significant impurity [25]. Absorption bands near 1600 cm^{-1} and 3411 cm^{-1} represent O-H stretching and bending mode of vibrations of water, respectively.

The X-ray diffraction patterns of samples are shown in Fig. 4. The diffraction patterns of samples match quite well with hexagonal structure of ZnO using the standard data (JCPDS-79-0206) [26,27] without any impure phases corresponding to the Co and Ni or their oxides. It seems that the doping with Co^{2+} and Ni^{2+} ions has no appreciable effect on the crystal phase of ZnO [28].

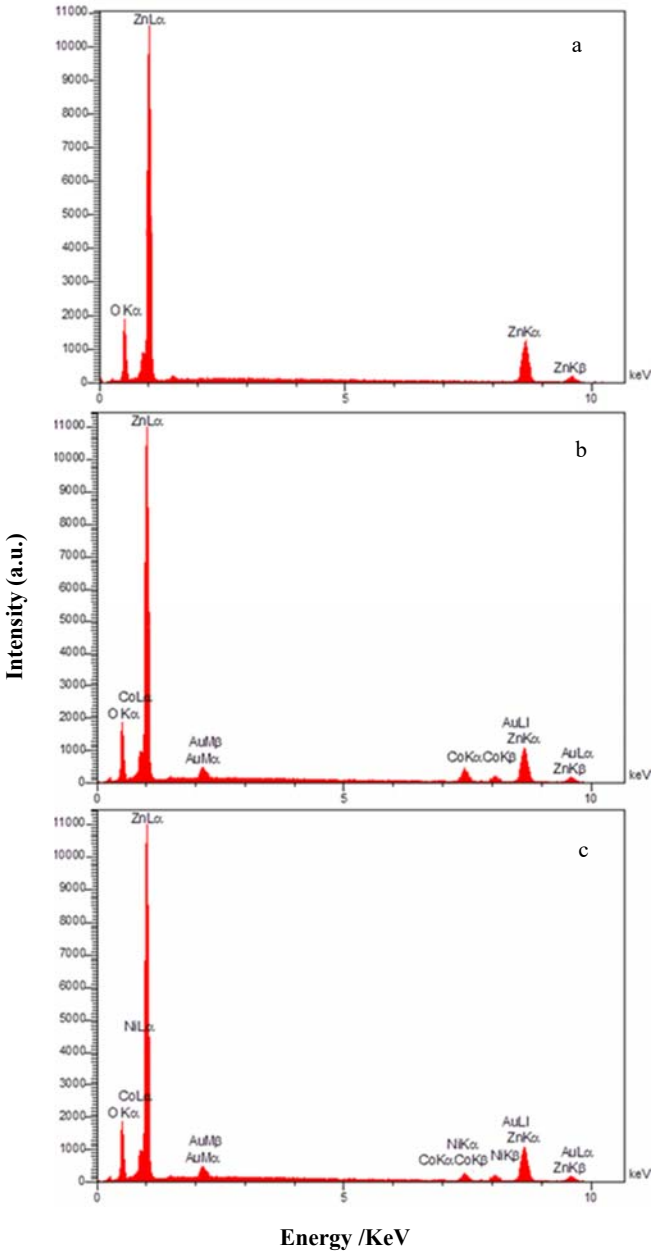

Fig. 2. Typical EDAX pattern obtained for the ZnO, Co-ZnO and Co-Ni-ZnO NPs.

Table 1. EDX data of the samples.

Element	ZnO	$Zn_{0.99}Co_{0.01}O$	$Zn_{0.99}Co_{0.005}Ni_{0.005}O$
O K	36.63	35.01	35.72
Co K	-	0.89	0.46
Ni K	-	-	0.42
Zn K	63.37	64.10	63.4
Total	100.00	100.00	100.00

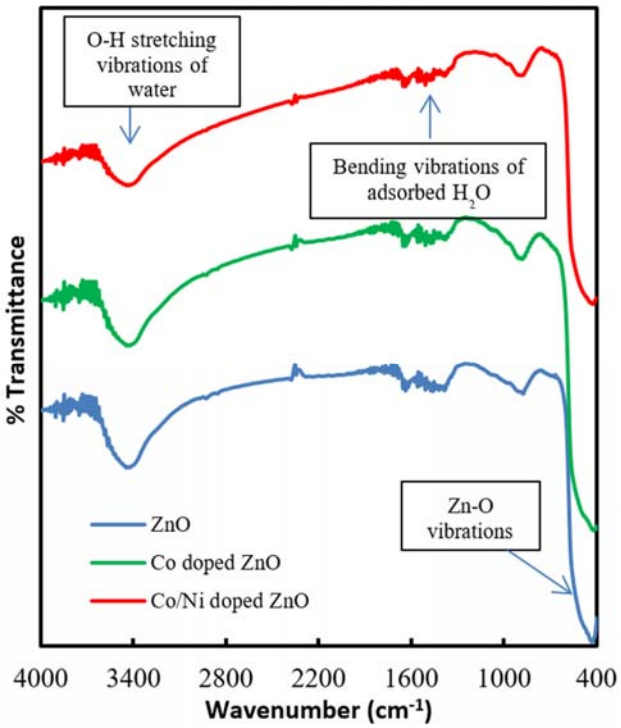

Fig. 3. FT-IR spectra of ZnO, Co-ZnO and Co-Ni-ZnO NPs.

The lattice parameters (a and c) of samples are found using the following equation [21].

$$\frac{1}{d^2} = \frac{4}{3}\left(\frac{h^2+kh+k^2}{a^2}\right) + \frac{l^2}{c^2} \quad (1)$$

Where h, k and l are Miller indexes and d is the distance between adjacent lattice planes in the crystal.

Table 2 shows the calculated lattice parameters of the samples. Although doping does not alter the crystal structure which causes the change of lattice constant as evidenced by the [002] peak position shift. The c-axis constant [d (002)] decreased by 0.30% and 0.24% respectively for the Co-ZnO and Co-Ni-ZnO NPs, which is consistent with the substitution of Zn by the dopants [21,29].

The crystalline size is determined by applying Debye-Scherrer formula [30]:

$$D = k\lambda/\beta\cos\theta \quad (2)$$

Where D is the crystalline size, b is the full width half maximum (FWHM) of the 2θ peak, K is the shape of particle factors (it equals to 0.89), θ and l are the incident of angle and wavelength of the X-rays, respectively. The average crystalline size of ZnO, Co-ZnO and Co-Ni-ZnO NPs associated with all the diffraction peaks was estimated about 19.90, 17.80 and 16.50 nm, respectively. The results revealed that there are reduced in the crystalline size of ZnO after doping with Co and Ni.

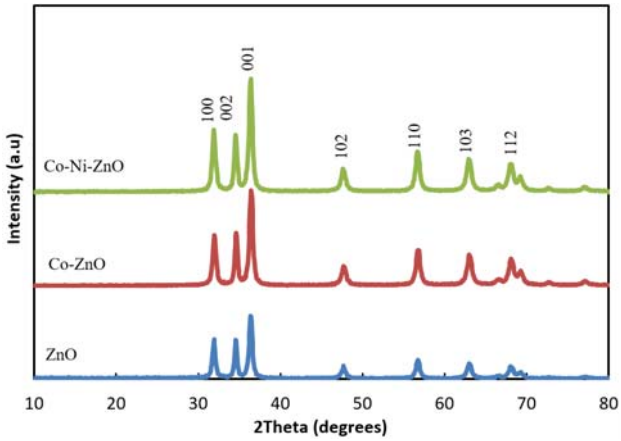

Fig. 4. XRD spectra of ZnO, Co-ZnO and Co-Ni-ZnO NPs.

It may be due to the small grain growth of doped ZnO nanoparticles as comprised with pure ZnO nanoparticles. This indicates that the doped ZnO has smaller lattice parameters and reduction in average crystallite size, which might originate from the smaller ion radius of Co^{2+} (0.058 nm) and Ni^{2+} ion (0.055 nm) compared to Zn^{2+} (0.060 nm) [31]. In addition, it can be seen that with the increasing of dopant cation, locations of the measured diffraction peaks do not change significantly but the relatively intensity of diffraction peaks increase obviously, which might be due to the increase in the lattice order and reduced strain, by Co^{2+} and Ni^{2+} substitution [5].

3.2. Optical properties of samples

To confirm the optical properties of the ZnO, Co-ZnO and Co-Ni-ZnO NPs, the UV-Vis absorption spectra were also recorded and the results are presented in Fig. 5. [32]. It can be clearly seen that in all samples, the sharp absorption edge at the wavelength around 370 nm can be assigned to the intrinsic band gap absorption for the wurtzite hexagonal structure of ZnO.

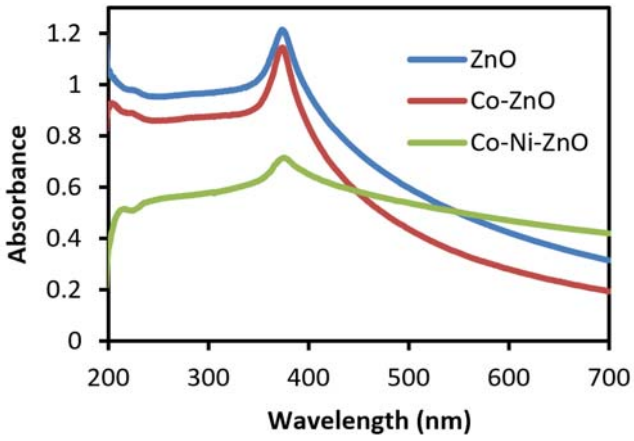

Fig. 5. UV-Vis absorption spectra of ZnO, Co-ZnO and Co-Ni-ZnO NPs.

Comparison of the UV-Vis spectra of undoped and doped ZnO in the maximum of the absorbance band shows slight red shifts (0.5 nm) due to cobalt doping and more red shift (2.5 nm) due to cobalt and nickel co-doping. The wavelengths of maximum absorbance for each nanostructure sample are listed in Table 2.

The absorption coefficients of samples were investigated by Tauc's approach and the optical band gap of the ZnO NPs was calculated using the following equation [33]:

$(\alpha h\nu)^2=C\ (h\nu-E_g)$

Where α is the absorption coefficient, C is a constant, $h\nu$ is the photon energy and E_g is the band gap. Fig. 6 shows the Tauc plots of samples. Extrapolation of the linear region of Tauc plot gives a band gap.

Comparing the Co-ZnO NPs to ZnO, the band gap slightly reduced, but with the Ni doping in the Co-Ni-ZnO NPs, the band gap significantly reduced (Table 2), because the excess carriers provided by Ni doping can fill some energy levels on the edge of conduction band and cause the transition energy decrease [21,22]. Furthermore, sp–d exchange interactions are responsible for the band gap variations in Co-Ni- ZnO sample. Energy diagram of samples is shown in Fig. 7. The results revealed that Co-Ni co-doping resulted in a widening of the band gap. It can be deduced that Co^{2+} and Ni^{2+} ions have entered into the lattice of ZnO [17], which was in accordance with the XRD results.

Room temperature PL spectra of the samples are shown in Fig. 8, in which all samples have two peaks around 380 nm (near-band edge emission (NBE), which come from the recombination of the free excited electrons and holes) and 570 nm (deep level emission (DLE) mediated by oxygen vacancies and other defects). Since PL emission is the result of the recombination of excited electrons and holes, the lower PL intensity of the sample indicates a lower recombination rate of excited electrons and holes [34-36].

The PL spectra of the samples show that the intensity of the deep level emission (DLE) band for the ZnO NPs is higher than that of other samples. It can be deduced that oxygen vacancies and other defects in ZnO are higher than those in other samples. Sebastian *et al.* [16] showed that the photoluminescence (PL) emission for the Co, Ni co-doping ZnO is almost quenched, indicating that O vacancies are filled up in the sample. On the other hand, the enhancement of PL intensity with the Co^{2+} doping was reported by Wang et al. [37], who attributed this result to the increase of defects and oxygen vacancies [20]. Moreover, Fig. 8 shows that in Co-Ni-ZnO NPs, the near-band edge emission (NBE) peak intensity decreases, probably due to less recombination rate of the free excited electrons and holes.

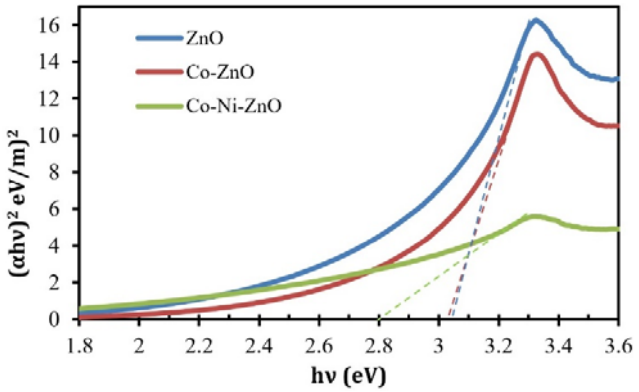

Fig. 6. Tauc plots of ZnO, Co-ZnO and Co-Ni-ZnO NPs.

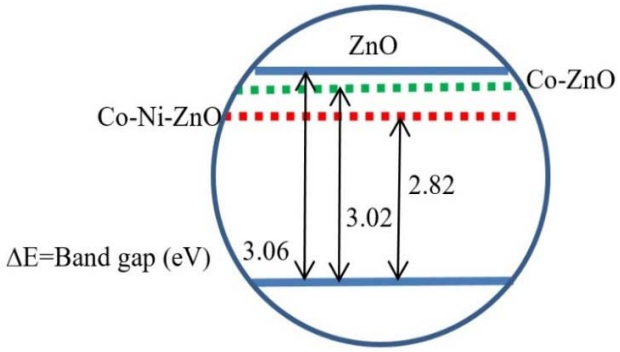

Fig. 7. Energy diagram of ZnO, Co-ZnO and Co-Ni-ZnO NPs.

Table 2. Peak position, band gap, lattice constants and photocatalytic activity of samples.

Samples	a (100)	c (002)	Wavelength (nm)	Band gap (eV)	Degradation in 120 min	k (min^{-1})
ZnO	3.2475	5.2059	373.5	3.06	60%	0.0083
Co-ZnO	3.2377	5.1899	374.0	3.02	69%	0.0104
Co-Ni-ZnO	3.2388	5.1933	376.0	2.82	99%	0.0249

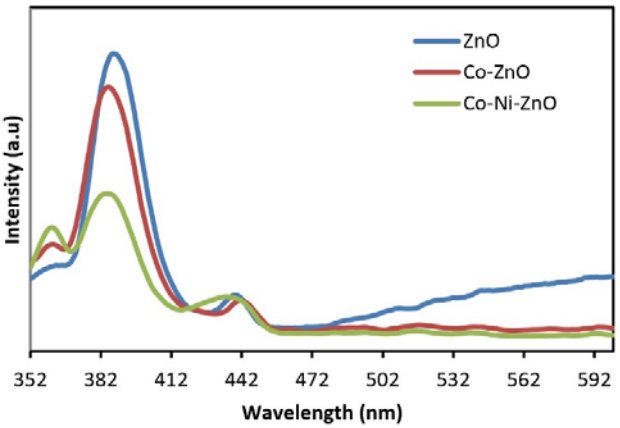

Fig. 8. The PL spectra of ZnO, Co-ZnO and Co-Ni-ZnO NPs.

3.3. Photocatalytic activity

In order to evaluate the photocatalytic activity of the samples, photodegradation of methyl orange (MO) under UV light irradiation was performed in the presence of samples at room temperature and the results are shown in Fig. 9. The absorption peaks corresponding to methyl orange molecule (Fig. 9 (a)) decrease gradually as the exposure time increases. No new absorption bands appear in either visible or ultraviolet regions, which indicates the photodegradation of methyl orange to smaller fragments [38].

Fig. 9 (c) shows the -ln(C/C_0) versus reaction time curves of the photocatalytic degradation of MO over Co-Ni-ZnO photocatalyst. The kinetic data of the photocatalytic degradation of MO over Co-Ni-ZnO fit well to the apparent first-order reaction kinetics as shown in Fig. 8b. The apparent first-order reaction rate constant (k) calculated from the slopes of these curves for pure and doped ZnO is shown in Table 1.

As observed in Fig. 9 (b and c), cobalt and nickel doping improved photocatalytic activity of ZnO. Moreover Co-Ni-ZnO NPs showed highest photocatalytic activity showing that the doping of Ni can significantly improve the photocatalytic efficiency of Co-ZnO [17] which is in agreement with the PL analysis. The enhancement of the co-doping on the photocatalytic activity of ZnO has not been well understood. According to the fact that doping with Co^{2+} alone has a little effect on the photocatalytic, we think that there might exist a cooperative enhancement on the activity in the co-doping system. The presence of Co and Ni traps the electron from the conductance band (CB) of ZnO simultaneously, which suppresses the photo-excited electron-hole recombination. This enhances the photocatalytic activity of Co-Ni-ZnO due to a synergistic effect between Co and Ni [39].

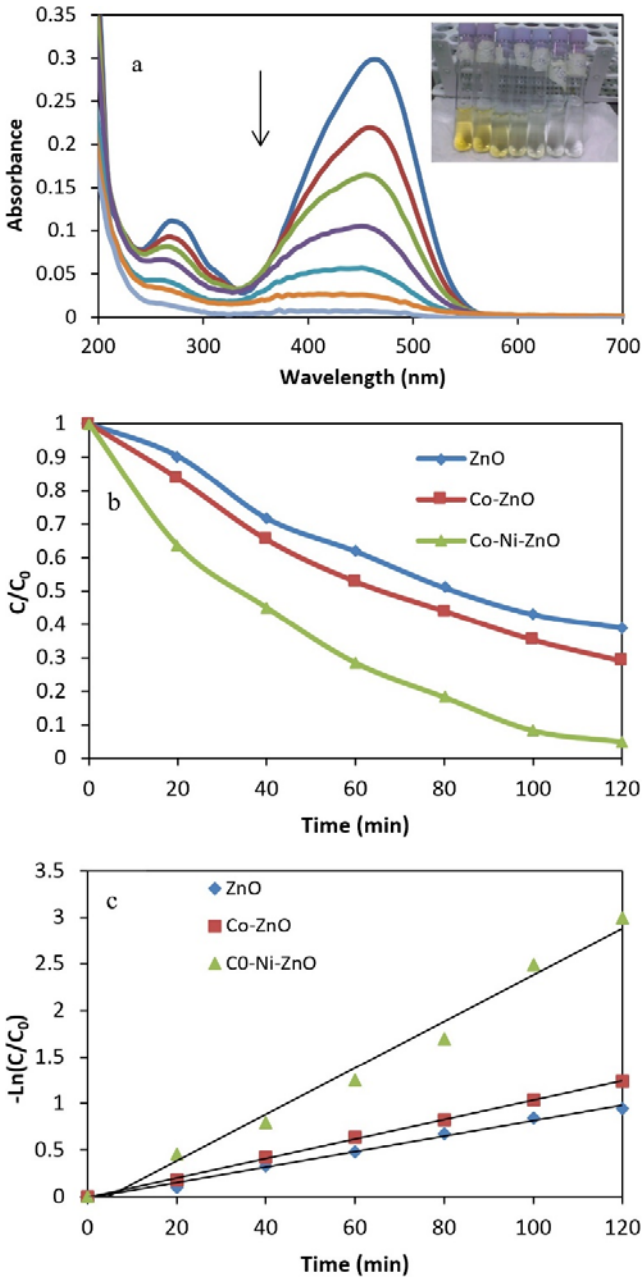

Fig. 9. (a) UV-vis spectra of the aqueous solutions of MO dye after UV irradiation for different time periods (0-120 min) in the presence of Co-Ni-ZnO, (b) Photodegradation of methyl orange (MO), (c) Typical ln(C/C_0) versus irradiation time plots using Co-Ni-ZnO.

3.4 Reusability of Co-Ni–ZnO

The reusability of the photocatalyst (Co-Ni-ZnO) is also an important factor for practical applications. Photocatalytic experiments were performed using the same catalyst. The photodegradation percentages of MO for the four successive cycling of Co-Ni-ZnO are 99%, 92%, 88% and 85%, respectively. The slight decrease in the photocatalytic activity after four cycles is ascribed to the loss of photocatalyst during washing.

4. Conclusion

Co-Ni-ZnO NPs were successfully synthesized through a facile one-pot sonochemical method. XRD results revealed that all synthesized samples showed a hexagonal wurtzite ZnO structure. Also, Co and Ni ions were successfully doped in to ZnO. In addition, XRD results indicate that the doped ZnO has smaller lattice parameters and reduction in average crystallite size. UV-Vis absorption spectra showed a red shift in doped sample compared to ZnO. The observed red shift of energy gap is explained by sp–d exchange interactions between the band electrons and the localized d-electrons of the Co^{2+} and Ni^{2+} ions. The PL spectra of samples showed less recombination rate of the free excited electrons and holes for the Co-Ni-ZnO NPs. The Co-Ni-ZnO showed an efficient photocatalyst in photodegradation of MO compared with Co-ZnO following the Co and Ni synergistic effect.

Acknowledgements

The authors are thankful to Iran National Science Foundation (INSF) for supporting this project numbered 90005627.

References

[1] C. Karunakaran, R. Dhanalakshmi, Radiat. Phys. Chem. 78 (2009) 8-12.
[2] I. Y.-Y. Bu, Superlattices Microst. 86 (2015) 36-42.
[3] M. Qamar, Q. Drmosh, M. I. Ahmed, M. Qamaruddin, Z. H. Yamani, Nanoscale Res. Lett. 10 (2015) 1-6.
[4] K. Vignesh, M. Rajarajan, A. Suganthi, J. Ind. Eng. Chem. 20 (2014) 3826-3833.
[5] M. Bordbar, S.M. Vasegh, S. Jafari, A.Y. Faal, Iran. J. Catal. 5 (2015) 135-141.
[6] A.B. Gomi, V. Ashayeri, Iran. J. Catal. 2 (2012) 135-140.
[7] M.H. Habibi, E. Askari, Iran. J. Catal. 1 (2011) 41-44.
[8] A. Nezamzadeh-Ejhieh, Z. Banan, Iran. J. Catal. 2 (2012) 79-83.
[9] A. Nezamzadeh-Ejhieh, M. Khorsandi, Iran. J. Catal. 1 (2011) 99-104.
[10] H.R. Pouretedal, M. Ahmadi, Iran. J. Catal. 3 (2013) 149-155.
[11] A.F. Shojaei, K. Tabatabaeian, M.A. Zanjanchi, H.F. Moafi, N. Modirpanah, J. Chem. Sci. 127 (2015) 481-491.
[12] E. Evgenidou, I. Konstantinou, K. Fytianos, I. Poulios, T. Albanis, Catal. Today 124 (2007) 156-162.
[13] J. Xie, H. Wang, M. Duan, L. Zhang, Appl. Surf. Sci. 257 (2011) 6358-6363.
[14] D. Jyothi, P.A. Deshpande, B.R. Venugopal, S. Chandrasekaran, G. Madras, J. Chem. Sci. 124 (2012) 385-393.
[15] T. Vinodkumar, D.N. Durgasri, S. Maloth, B.M. Reddy, J. Chem. Sci. 127 (2015) 1145-1153
[16] K.C. Sebastian, M. Chawda, L. Jonny, D. Bodas, Mater. Lett. 64 (2010) 2269-2272.
[17] X. Zhang, S. Dong, X. Zhou, L. Yan, G. Chen, S. Dong, D. Zhou, Mater. Lett. 143 (2015) 312-314.
[18] M. Ashokkumar, S. Muthukumaran, Opt. Mater. 37 (2014) 671-678.
[19] C. Xu, L. Cao, G. Su, W. Liu, X. Qu, Y. Yu, J. Alloys Compd. 497 (2010) 373-376.
[20] F.C. Romeiro, J.Z. Marinho, S.C.S. Lemos, A.P. de Moura, P.G. Freire, L.F. da Silva, E. Longo, R.A.A. Munoz, R.C. Lima, J. Solid State Chem. 230 (2015) 343-349.
[21] J. Zhao, L. Wang, X. Yan, Y. Yang, Y. Lei, J. Zhou, Y. Huang, Y. Gu, Y. Zhang, Mater. Res. Bull. 46 (2011) 1207-1210.
[22] B. Khodadadi, M. Bordbar, Iran. J. Catal. 6 (2016) 37-42.
[23] H.-Y. Zhu, L. Xiao, R. Jiang, G.-M. Zeng, L. Liu, Chem. Eng. J. 172 (2011) 746-753.
[24] A. Aslani, M. R. Arefi, A. Babapoor, A. Amiri, K. Beyki-Shuraki, Appl. Surf. Sci. 257 (2011) 4885-4889.
[25] C.K. Ghosh, S. Malkhandi, M.K. Mitra, K.K. Chattopadhyay, J. Phys. D: Appl. Phys. 41 (2008) 245113-245113.
[26] X. Zhou, Y. Li, T. Peng, W. Xie, X. Zhao, Mater. Lett. 63 (2009) 1747-1749.
[27] R. Saravanan, S. Karthikeyan, V.K. Gupta, G. Sekaran, V. Narayanan, A. Stephen, Mater. Sci. Eng. C 33 (2013) 91-98.
[28] N.V. Kaneva, D.T. Dimitrov, C.D. Dushkin, Appl. Surf. Sci. 257 (2011) 8113-8120.
[29] J.B. Cui, U.J. Gibson, Appl. Phys. Lett. 87 (2005) 133108.
[30] M. Bordbar, T. Alimohammadi, B. Khoshnevisan, B. Khodadadi, A. Yeganeh-Faal, Int. J. Hydrogen Energy 40 (2015) 9613-9620.
[31] M. Ram, G.S. Arya, K. Parmar, R.K. Kotnala, N.S. Negi, Int. J. Adv. Res. Technol. 8 (2015) 329-336.
[32] C. Liu, Z. Liu, Y. Li, Z. Liu, Y. Wang, L.E, J. Ya, N. Gargiulo, D. Caputo, Mater. Sci. Eng. B 177 (2012) 570-574.
[33] M. Bordbar, B. Khodadadi, N. Mollatayefe, A. Yeganeh-Faal, J. Appl. Chem. 8 (2013) 43-48.
[34] Q. Li, Z. Kang, B. Mao, E. Wang, C. Wang, C. Tian, S. Li, Mater. Lett. 62 (2008) 2531-2534.
[35] T. Long, K. Takabatake, S. Yin, T. Sato, J. Cryst. Growth 311 (2009) 576-579.
[36] J. Majeed, O.D. Jayakumar, B.P. Mandal, H.G. Salunke, R. Naik, A. K. Tyagi, J. Alloys Compd. 597 (2014) 95-100.
[37] B. Wang, C. Xia, J. Iqbal, N. Tang, Z. Sun, Y. Lv, L. Wu, Solid State Sci. 11 (2009) 1419-1422.
[38] D. Sridevi, K.V. Rajendran, Int. J. Nanopart. 4 (2011) 381-388.
[39] H.F. Moafi, M.A. Zanjanchi, A.F. Shojaie, J. Nanosci. Nanotechnol. 14 (2014) 7139-7150.